First-principles study of atomic and electronic structures of 60° perfect and 30°/90° partial glide dislocations in CdTe

Kyoung E. Kweon,* Daniel Åberg, and Vincenzo Lordi†
Lawrence Livermore National Laboratory, Livermore, California 94550, USA
(Received 30 October 2015; revised manuscript received 1 April 2016; published 16 May 2016)

The atomic and electronic structures of 60° glide perfect and 30°/90° glide partial dislocations in CdTe are studied using combined semi-empirical and density functional theory calculations. The calculations predict that the dislocation cores tend to undergo significant reconstructions along the dislocation lines from the singly-periodic (SP) structures, yielding either doubly-periodic (DP) ordering by forming a dimer or quadruply-periodic (QP) ordering by alternating a dimer and a missing dimer. Charge modulation along the dislocation line, accompanied by the QP reconstruction for the Cd-/Te-core 60° perfect and 30° partials or the DP reconstruction for the Cd-core 90° partial, results in semiconducting character, as opposed to the metallic character of the SP dislocation cores. Dislocation-induced defect states for the 60° Cd-/Te-core are located relatively close to the band edges, whereas the defect states lie in the middle of the band gap for the 30° Cd-/Te-core partial dislocations. In addition to the intracore charge modulation within each QP core, the possibility of intercore charge transfer between two different dislocation cores when they are paired together in the same system is discussed. The analysis of the electronic structures reveals the potential role of the dislocations on charge transport in CdTe, particularly in terms of charge trapping and recombination.

DOI: 10.1103/PhysRevB.93.174109

I. INTRODUCTION

Cadmium telluride (CdTe) and its alloy cadmium zinc telluride (CZT) have long been regarded as promising semiconductor materials for high-resolution, room temperature x-ray and γ-ray detectors, due to their high average atomic numbers, band gaps spanning the 1.4 to 1.7 eV range, and moderately high charge carrier mobilities and lifetimes [1,2]. However, their ultimate energy resolution has been largely limited by defects formed during crystal growth, including point defects, dislocations, and grain boundaries, because these defects often behave as charge trapping centers for electrons or holes and either induce recombination or delay carrier collection [3–7]. Among various defects, dislocations are of particular interest in CdTe, as they have been experimentally observed to cause defect states within the band gap and show a strong correlation between their spatial distributions and substantial charge trapping in devices excited by x rays [7–10]. However, as dislocations often are found decorated with impurities or Te-rich secondary phases (Te precipitates or inclusions) [5,7], it is difficult to determine experimentally whether the charge carrier trapping is primarily due to the dislocations themselves or their decorating defects. Thus, theoretical calculations are necessary to elucidate the specific role of dislocations on carrier trapping in Cd(Zn)Te, separated from the decorating defects.

Dislocations in a crystal are characterized by slip systems consisting of a slip plane and direction. In a zinc-blende crystal, slip preferentially occurs on close-packed {111} planes along a close-packed ⟨110⟩ direction [11]. One of the common dislocations belonging to the {111}⟨110⟩ slip system is the 60° perfect dislocation, where the angle between the Burgers vector (corresponding to the slip direction) and the dislocation line is 60° [12]. The 60° perfect dislocation often lowers its elastic strain energy by dissociating into two Shockley 30° and 90° partial dislocations with the formation of a stacking fault between them. Due to a low stacking fault energy [13], the dissociated partial dislocations are mainly observed in CdTe, but undissociated 60° dislocations are still experimentally found [14–17]. Thus both undissociated and dissociated dislocations are important to consider in CdTe to understand dislocation-induced defect levels. Also, note that for each dislocation, there are two different core types that are inherently nonstoichiometric (which we call "Cd-core" and "Te-core"), since the cores can be terminated by either Cd or Te atomic columns. The structures we study are inspired by experimentally observed 30° partial dislocation structures in CdTe [14,15,17].

In this work, we perform both semiempirical and density functional theory calculations to explore the structural and electronic properties of 60° perfect and 30°/90° partial dislocations in CdTe. With different {111} slip planes (narrowly spaced glide and widely spaced shuffle planes), undissociated 60° and dissociated 30°/90° dislocations belong to either the glide or shuffle set. For the dissociated 30°/90° partials, the glide set is generally considered the primary type, since low-energy stable stacking faults can only exist in the glide-set plane [18]. For the undissociated 60° perfect dislocation, the dominant set is less clear, but it is generally believed that both sets are not mutually exclusive and their relative concentrations are dependent on the experimental conditions [18]. Here, we only consider dislocations of the glide set, since we focus on super-periodic dislocation core reconstructions along the dislocation line direction. The directionality of broken bonds that form the dislocation core lies in the plane perpendicular to the line direction for the shuffle set (on the $\{1\bar{1}0\}$ plane), so that reconstructions occur in that plane rather than along the dislocation line; for the glide set, the broken bonds

*kweon1@llnl.gov
†lordi2@llnl.gov

lie nearly on the {111} slip planes and many are oriented such that reconstructions along the dislocation line may be favored [19–23].

For each isolated 60° perfect and 30° and 90° partial dislocation (both Cd-core and Te-core in each case), we first examine dislocation core structures that are periodic with the lattice of the unit cell in the dislocation line direction ("singly-periodic"). We also find core reconstructions resulting in doubly- and quadruply-periodic ordering along the dislocation line direction and compare their energetics, atomic configurations, and electronic structures with those of the singly-periodic core. We find the quadruply-periodic reconstructed core structures are energetically the most favorable for the 60° perfect and 30° partial dislocations, leading to a preferred charge modulation along the dislocation line for overall neutral cores rather than charged metallic dislocation cores. A similar effect occurs for the 90° Cd-core partial, but in that case, a doubly-periodic core reconstruction that maintains overall neutrality is favored. In addition, we consider the effects of two different dislocation cores existing in the same system and discuss the possibility of intercore charge transfer. Based on the results, we evaluate the impact of dislocation-induced defects on charge transport in CdTe.

II. METHODS

We performed both semi-empirical and density functional theory (DFT) calculations to determine the energetics, atomic configurations, and electronic properties of the dislocation cores. Initially, single dislocations were introduced into large orthorhombic cells of ∼12 000 atoms with the y axis parallel to the $[1\bar{1}0]$ dislocation line direction and x and z axes parallel to the $[\bar{1}\bar{1}2]$ and [111] of the zinc-blende lattice, respectively. Each 60° perfect dislocation and 30° and 90° partial dislocation was constructed with Burgers vector $\frac{1}{2}[0\bar{1}1]$, $\frac{1}{6}[1\bar{2}1]$, and $\frac{1}{6}[\bar{1}\bar{1}2]$, respectively. The dimensions of the cell along the x, y, and z direction were $20 \times 1 \times 24$, with respect to each unit cell lattice vector. We applied free surface boundary conditions in the x-z plane, while periodic boundary conditions along the y direction to simulate an infinitely long dislocation line.

To relax the large initial dislocation structures, semiempirical calculations using a Stillinger-Weber potential [24] were carried out using the LAMMPS package [25] to take into account the long-range strain field around the dislocation cores. Then, a smaller model (∼150 atoms) was extracted from the large one for DFT calculations, and each Cd and Te dangling bond at the edge was passivated by a pseudohydrogen atom with a fractional charge of 1.5 or 0.5 electrons, respectively, to ensure charge balance, as shown in Fig. 1. A minimum vacuum separation of ∼11 Å was chosen to avoid interaction between replicated cells along the x and z directions. In addition, the smaller cell was quadrupled along the $[1\bar{1}0]$ dislocation line direction to examine structural relaxations along that direction, resulting in a model containing ∼750 atoms, including the pseudohydrogen atoms.

All DFT calculations were performed using the local density approximation (LDA) [26] and projector-augmented wave (PAW) approach [27] as implemented in the VASP code [28]. A plane-wave cutoff energy of 275 eV and a

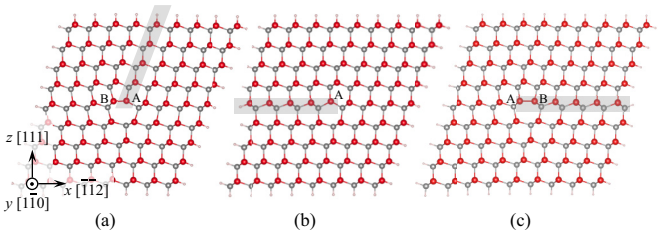

FIG. 1. Atomic structure models of the (a) 60° perfect, (b) 30° partial, and (c) 90° partial dislocations for DFT calculations, projecting along the $[1\bar{1}0]$ dislocation line direction. All dangling bonds at the edge atoms are passivated by pseudohydrogen atoms. The inserted half-plane in (a) and the stacking fault region in (b) and (c) are shaded. The selected core atoms are labeled as A and B. Here, Cd-core dislocations are shown for illustration. Red, gray, and small white balls represent Cd, Te, and pseudohydrogen atoms, respectively.

$1 \times 2 \times 1$ Monkhorst-Pack k-point mesh [29] were used for geometry optimization; for computing the corresponding electronic structure, the cutoff energy and the k-point mesh density were increased to 330 eV and a Γ-centered $1 \times 4 \times 1$ mesh, respectively. The valence electron configurations considered were $4d^{10}5s^2$ for Cd and $5s^25p^4$ for Te, with the remaining electrons frozen in pseudopotential cores. During the structural relaxations with DFT, the Cd and Te atoms of the outermost layer in the x-z plane were fixed to maintain the long-range strain field calculated from the large Stillinger-Weber-relaxed structures, while all remaining atoms including pseudohydrogens were fully relaxed until the residual forces on constituent atoms were smaller than 0.02 eV/Å.

III. RESULTS

A. 60° perfect dislocations

Figure 2 shows the geometries of possible Cd-core 60° glide dislocations, and the corresponding partial local electronic density of states (PLDOS) are shown in Fig. 3. First, as shown in Fig. 2(a), the core Cd atom (Cd_{A1}) is threefold coordinated

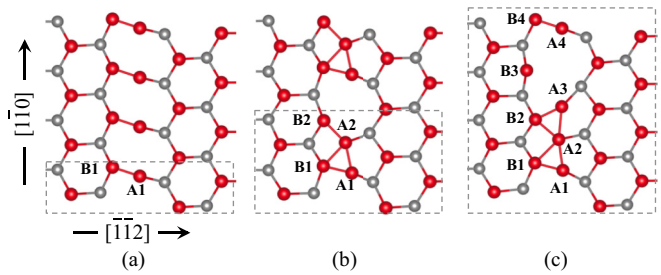

FIG. 2. Optimized configurations of a Cd-core 60° glide dislocation in the {111} glide plane. (a) The singly-periodic (SP) and the (b) doubly-periodic (DP) and (c) quadruply-periodic (QP) core structures along the $[1\bar{1}0]$ dislocation line direction. For comparison with the QP structure, the unit cell of SP and DP structure (indicated by the dashed box) is quadrupled and doubled, respectively, in the $[1\bar{1}0]$ direction. Important core Cd atoms in each unit cell are labeled as A and B with numbers, indicated. Red and gray balls represent Cd and Te atoms, respectively.

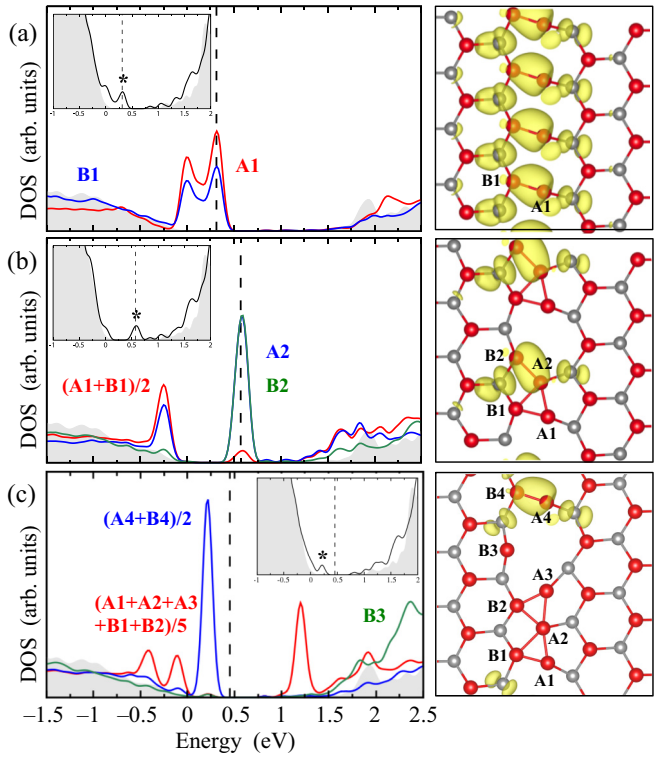

FIG. 3. (Left) Projected DOS onto the core Cd atoms and (right) band-decomposed charge density for the (a) SP, (b) DP, and (c) QP core structures for the Cd-core 60° glide dislocation. The energy zero is set to the top of the valence band of the pristine structure without a dislocation, and the Fermi level is indicated by vertical dashed lines; the band gap of the pristine CdTe structure is calculated to be 0.9 eV. The projected DOS onto the Cd atom in the pristine CdTe structure are shown as gray shaded areas for a reference. In the insets, the total DOS are shown by the black curves and the gray shaded areas indicate the total DOS for the pristine CdTe structure. The band-decomposed charge densities of core-related states within the band gap (indicated by asterisks in the total DOS plot in the insets) are plotted as isosurfaces set at 10% of the maximum value.

and bonded to the Cd_{B1} atom with a bond length of 2.65 Å, which is considerably shorter than the calculated Cd–Cd bond length of 2.88 Å for bulk Cd [30]; in this configuration, Cd_{A1} forms a nearly planar configuration with its three neighboring atoms. The core is a singly-periodic (SP) structure and the distance between neighboring Cd_{A1} atoms along the dislocation line is 4.54 Å; here, SP refers to the structure having a lattice vector along the dislocation line direction that equals a single unit vector of the zinc-blende lattice, as indicated by the dashed rectangular box in Fig. 2(a). According to the PLDOS and partial charge density calculations shown in Fig. 3(a), there is a partially filled defect state near the top of the valence band, which is predominantly derived from Cd_{A1} and Cd_{B1} states. It is worth noting that before forming the Cd_{A1}–Cd_{B1} bond, there are three broken Cd bonds at the core due to the inserted half-plane (one is from Cd_{B1} and the other two are from Cd_{A1}), and that forming the bond between Cd_{A1} and Cd_{B1} stabilizes these dangling bonds; in Fig. 2(a), all Cd and Te atoms except the core atoms are fourfold coordinated with one additional bond (not shown) oriented along the [111] direction. Since each broken Cd bond is associated with 0.5 electrons (e) (note that a Cd–Te bond is formed approximately by $0.5e$ from Cd and $1.5e$ from Te), the defect state corresponding to the Cd_{A1}–Cd_{B1} bonding state is partially occupied by $1.5e$, as illustrated by the band-decomposed charge density isosurface in Fig. 3(a).

The undercoordinated Cd_{A1} atoms drive the SP structure to undergo a reconstruction along the dislocation line by forming a bond between two neighboring Cd_{A1} atoms, yielding a doubly-periodic (DP) structure as shown in Fig. 2(b) with an energy gain of 0.34 eV/nm. In the DP structure, the Cd_{A1}–Cd_{A2} bond length is 2.87 Å, while the Cd_{A2} also forms a bond with Cd_{B1} with a bond length of 2.97 Å. As shown in Fig. 3(b), the DP reconstruction enables two three-quarter-filled states ($2 \times 1.5\,e$) to split into one fully filled ($2.0e$) and one half-filled ($1.0e$) state. The defect state associated with Cd_{A1}, Cd_{B1}, and Cd_{A2} in a three-center two-electron bond is fully occupied and merges into the valence band. On the other hand, the defect state involved in the Cd_{A2}–Cd_{B2} bonding lies near the middle of the band gap and is half-filled; with the decreased charge on the Cd–Cd bonding state (from $1.5e$ to $1.0e$), the Cd_{A2}–Cd_{B2} bond length is noticeably elongated to 2.83 Å compared to 2.65 Å for the SP structure. Similar DP reconstructions along the dislocation line have also been proposed for 60° dislocations in Si and diamond [19,21].

Since there are still partially filled states in the band gap, we further examine possible reconstruction to a quadruply-periodic (QP) structure generated initially by combining a dimer and a missing dimer along the dislocation line. After relaxation, the core Cd_{A1}, Cd_{A2}, and Cd_{A3} atoms in the QP structure form a trimer along the dislocation line, while Cd_{A4} remains threefold coordinated as in the SP core [see Fig. 2(c)]. We also note that the core Cd_{A1}–Cd_{A2}–Cd_{A3} trimer exhibits strong interactions with Cd_{B1} and Cd_{B2} resulting in the formation of two triangular Cd clusters on the {111} glide plane, similar to bulk Cd atoms in the hexagonal close packed structure [30]. On the other hand, the remaining Cd_{B3} adopts a nearly planar sp^2 configuration with its three Te neighbors; such a planar $CdTe_3$ configuration is reminiscent of the atoms surrounding a Te vacancy in CdTe [6,31,32]. Our calculation predicts that the QP structure is 0.58 eV/nm lower in energy compared to the SP structure.

As shown in Fig. 3(c), the QP reconstruction converts four three-quarter-filled states ($4 \times 1.5\,e$) into three fully occupied defect states ($3 \times 2.0\,e$). Two occupied defect states lying below the valence-band edge are associated with the two Cd triangles (Cd_{A1}–Cd_{A2}–Cd_{B1} and Cd_{A2}–Cd_{A3}–Cd_{B2}), each of which serves as a three-center/two-electron Cd bond. The remaining occupied Cd_{A4}–Cd_{B4} bonding state appears slightly above the top of the valence band. The empty antibonding states for the three-center/two-electron Cd bonds are situated slightly above the conduction-band edge. Of particular note is that the charge density at the QP dislocation core is no longer uniformly distributed along the dislocation line, and rather charge modulation occurs along the dislocation line.

Next, we examine the corresponding configurations of the Te-core 60° glide dislocations in a similar manner as the Cd-core cases analyzed above. Figure 4(a) shows the SP configuration with the threefold-coordinated Te_{A1} atom

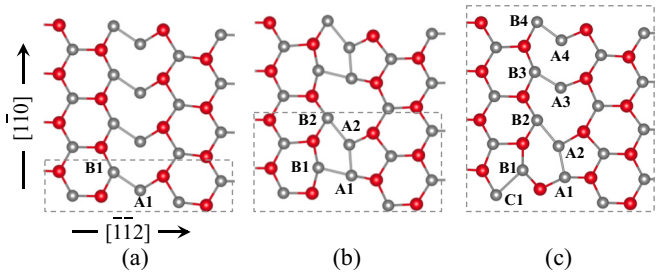

FIG. 4. Optimized configurations of a Te-core 60° glide dislocation in the {111} glide plane. (a) The SP (b) DP and (c) QP core structures along the [1$\bar{1}$0] dislocation line direction. Important core Te atoms in each unit cell are labeled as A and B with numbers, indicated. Red and gray balls represent Cd and Te atoms, respectively.

forming a bond with the Te_{B1} atom with a bond length of 2.98 Å, while exhibiting a distorted tetrahedral configuration. Since each broken Te bond is associated with 1.5e, there are 4.5e available at the core before forming the bond between Te_{A1} and Te_{B1}. Our analysis shows that the Te_{A1}–Te_{B1} bond utilizes 2.5e, while the remaining 2.0e reside on a lone pair state of Te_{A1} that appears slightly below the valence-band edge. (The occurrence of a similar lone pair state on a chalcogen atom has been recently suggested for S atoms at the interface between a Si nanoparticle and ZnS [33].) Among the 2.5e in the Te_{A1}–Te_{B1} bond, 2.0e occupy the bonding state, while the remaining 0.5e partially fills the antibonding state located in the middle of the band gap, as shown in Fig. 5(a). Due to partial filling of the antibonding state, the Te_{A1}–Te_{B1} bond length is slightly longer than the calculated bulk Te–Te single-bond length of 2.90 Å [34].

With structural relaxation along the dislocation line, the Te_{A1}–Te_{A2} dimer is formed in the DP structure, as depicted in Fig. 4(b), with an energy gain of 0.07 eV/nm with respect to the SP structure. The bond length of 2.89 Å for the Te_{A1}–Te_{A2} bond is comparable to the bulk Te–Te single-bond length. The relatively small energy gain can be attributed to the stability of the tetrahedral coordination of the threefold Te_{A1} atom with the lone pair in the SP structure. The calculated PLDOS in Fig. 5(b) shows that two one-quarter-filled states (2×0.5 e) split into a one-half-filled (1.0e) and a fully empty state (0.0e). The Te_{A1}–Te_{B1} antibonding state, located near the middle of the band gap, is half-filled, increasing the Te_{A1}–Te_{B1} bond length to 3.18 Å. On the other hand, the Te_{A1}–Te_{A2} antibonding state is located slightly above the conduction-band edge.

The QP structure is obtained by alternately forming a dimer along the dislocation line of the SP structure, as shown in Fig. 4(c), and is 0.22 eV/nm lower in energy compared to the SP structure. Note that the Te_{A1}–Te_{B1} bond is broken, while new bonds form with neighboring Cd or Te atoms. The PLDOS in Fig. 5(c) shows that there are one fully filled state and three empty states near the band gap. Evidently, the partial charges associated with the Te_{A3}–Te_{B3} and Te_{A4}–Te_{B4} antibonding states are transferred to the newly formed Te_{B1}–Te_{C1} antibonding state, as shown in the band decomposed charge density plot in Fig. 5(c). As a result, the Te_{A3}–Te_{B3} and Te_{A4}–Te_{B4} bonds have nearly single-bond character with lengths of 2.81 and 2.82 Å, respectively.

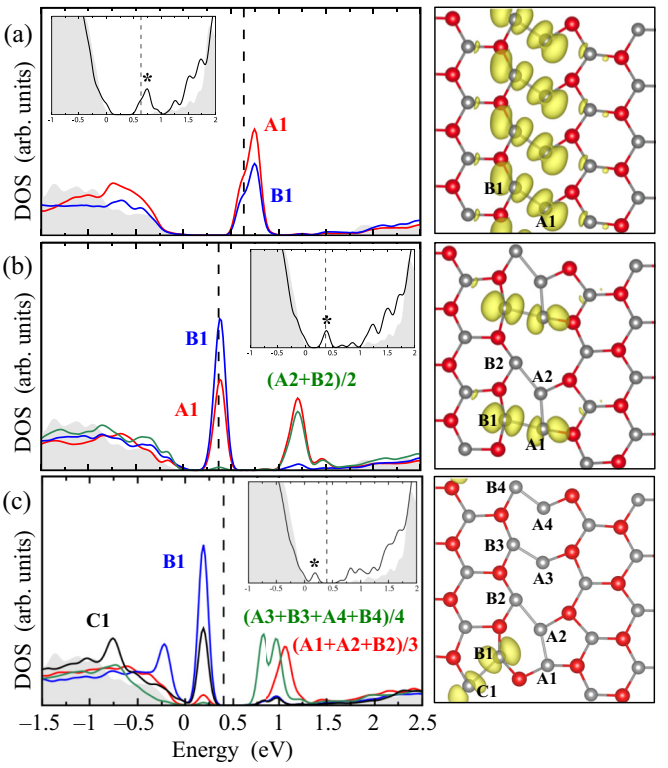

FIG. 5. (Left) Projected DOS onto the core Te atoms and (right) band-decomposed charge density for the (a) SP, (b) DP, and (c) QP core structures for the Te-core 60° glide dislocation. The energy zero is set to the top of the valence band of the pristine structure without a dislocation, and the Fermi level is indicated by vertical dashed lines. The projected DOS onto the Te atom in the pristine CdTe structure are shown as gray shaded areas for a reference. In the insets, the total DOS are shown by the black curves and the gray shaded areas indicate the total DOS for the reference dislocation-free CdTe structure. The band-decomposed charge densities of core-related states within the band gap (indicated by asterisks in the total DOS plot in the insets) are plotted as isosurfaces set at 10% of the maximum value.

Based on our calculations, the QP reconstructions are predicted to be the most stable for both the Cd-core and Te-core 60° glide dislocations, among the three core configurations examined in this work. (Since the electron pairing drives the QP reconstructions, larger periodicities are not expected to occur; the local structural motifs in the QP configurations therefore should represent any longer-range non-periodic arrangement along the dislocation line.) For the QP-reconstructed Cd-core 60° glide dislocation, the absence of any deep defect states suggests that the Cd-core dislocations might not act as charge trap or recombination centers. However, the QP-reconstructed Te-core 60° glide dislocation exhibits empty deep gap states associated with the core Te–Te bond, which can trap electrons and deteriorate charge transport, unlike the case for the Cd-core dislocations.

B. 30° partial dislocations

Here, we investigate the core configurations and the electronic structures of the 30° glide partial dislocation, which is one of the two partials from dissociation of the 60° glide

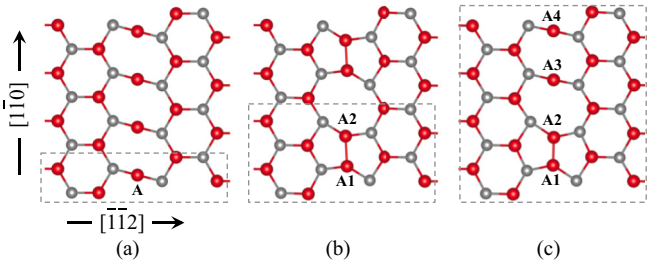

FIG. 6. Optimized configurations of a Cd-core 30° partial dislocation in the {111} glide plane. Important core Cd atoms in each unit cell are labeled as A with numbers, indicated. Red and gray balls represent Cd and Te atoms, respectively.

dislocation. First, for the Cd-core case, the geometry of the SP structure is presented in Fig. 6(a). The core Cd_{A1} atom is threefold coordinated and possesses a sp^2-like configuration with bond angles of nearly 120°. As shown in Fig. 7(a), the defect state appears very close to the bottom of the conduction band and is hybridized with the largely dispersed conduction-band edge. Thus the $0.5e$ from the one broken Cd bond from Cd_{A1} fills the bottom of the conduction band, and the corresponding charge spreads over many Cd sites [see Fig. 7(a)] near Cd_{A1}. The results for the geometries and electronic structures of the SP structure are very similar to those from previous studies [14,35].

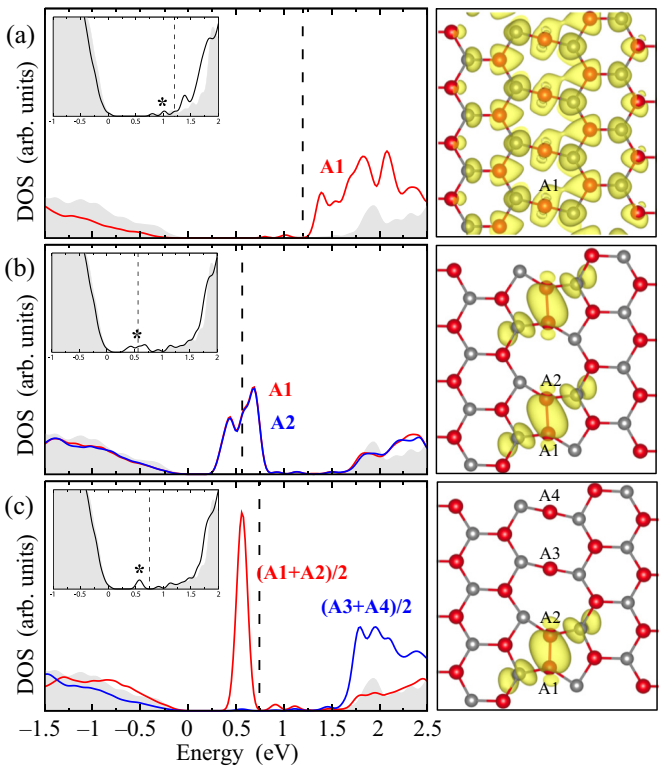

FIG. 7. (Left) Projected DOS onto the core Cd atoms and (right) band-decomposed charge density for the (a) SP, (b) DP, and (c) QP core structures for the Cd-core 30° glide dislocation. The energy zero is set to the top of the valence band of the pristine structure without a dislocation, and the Fermi level is indicated by vertical dashed lines. The projected DOS onto the Cd atom in the pristine CdTe structure are shown as gray shaded areas for a reference. In the insets, the total DOS are shown by the black curves and the gray shaded areas indicate the total DOS for the reference dislocation-free CdTe structure. The band-decomposed charge densities of core-related states within the band gap (indicated by asterisks in the total DOS plot in the insets) are plotted as isosurfaces set at 10% of the maximum value.

When two Cd atoms form a bond along the dislocation line, the Cd-core SP structure reconstructs to the DP structure shown in Fig. 6(b) with an energy gain of 0.24 eV/nm. As depicted in Fig. 6(b), the Cd_{A1}–Cd_{A2} bond length is 2.87 Å, which is very close to the calculated 2.88 Å in bulk Cd [30]. The calculated PLDOS in Fig. 7(b) shows that there is a one-half-filled state ($1.0e$) in the middle of the band gap. This defect state corresponds to the bonding state of the Cd–Cd dimer as also evidenced by the localized charge on the Cd_{A1}–Cd_{A2} bond shown in Fig. 7(b).

We find that the Cd-core DP structure can further reconstruct to a QP structure with undimerized core Cd atoms along the dislocation line as shown in Fig. 6(c), with an energy gain of 0.15 eV/nm compared to the DP structure (0.39 eV/nm lower in energy than the SP structure). According to the PLDOS, the Cd_{A1}–Cd_{A2} bond-related state lies in the middle of the band gap and $2.0e$ occupy this defect state, while no other defect states appear within the band gap. This indicates that the Cd_{A1}–Cd_{A2} bonding state becomes fully occupied by additionally donated $0.5e$ from each sp^2-like Cd_{A3} and Cd_{A4} atom [see the isosurface of the band-decomposed charge density in Fig. 7(c)], resulting in the shortened Cd_{A1}–Cd_{A2} bond length of 2.65 Å. Similar structural relaxation also has been suggested for the Te vacancy in CdTe, in which the four threefold-coordinated Cd atoms resulting from the missing Te atom reconfigure to form one Cd–Cd bond leaving two threefold-coordinated Cd atoms with sp^2 configuration [31].

In Fig. 8, the core configurations for the Te-core 30° glide partial dislocation are presented. In the SP structure, the threefold-coordinated Te_{A1} exhibits a trigonal pyramidal configuration with its neighboring Cd atoms. The PLDOS in Fig. 9(a) demonstrates that the defect state lies just above the top of the valence band and is partially empty since only $1.5e$ are contributed from one broken Te_{A1} bond (corresponding equivalently to a 0.5 hole state). The partially empty state is substantially localized on the Te_{A1} atom with mainly p-like character. As shown in the band decomposed charge density

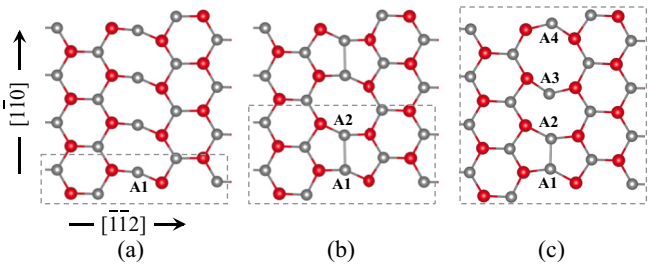

FIG. 8. Optimized configurations of a Te-core 30° partial dislocation in the {111} glide plane. Important core Te atoms in each unit cell are labeled as A with numbers, indicated. Red and gray balls represent Cd and Te atoms, respectively.

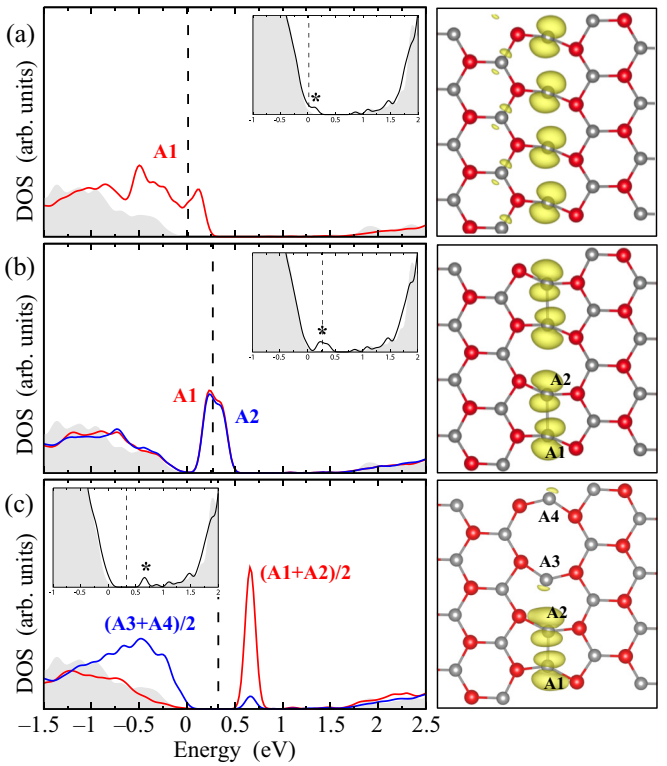

FIG. 9. (Left) Projected DOS onto the core Te atoms and (right) band-decomposed charge density for the (a) SP, (b) DP, and (c) QP core structures for the Te-core 30° glide dislocation. The energy zero is set to the top of the valence band of the pristine structure without a dislocation, and the Fermi level is indicated by vertical dashed lines. The projected DOS onto the Te atom in the pristine CdTe structure are shown as gray shaded areas for a reference. In the insets, the total DOS are shown by the black curves and the gray shaded areas indicate the total DOS for the reference dislocation-free CdTe structure. The band-decomposed charge densities of core-related states within the band gap (indicated by asterisks in the total DOS plot in the insets) are plotted as isosurfaces set at 10% of the maximum value.

plot in Fig. 9(a), this state is oriented perpendicularly to the plane of neighboring three Cd atoms; this result is similar with a previously reported calculation for Te-core 30° glide partial dislocations [35]. Also, a similar feature has been suggested for the Si or C core atoms of the 30° glide partial dislocations in SiC [36].

With Te–Te dimer formation along the dislocation line, the DP structure in Fig. 8(b) is formed with an energy gain of 0.15 eV/nm over the SP structure. Here, 3.0e in the Te–Te bond give rise to a half-filled antibonding state as well as a fully occupied bonding state, resulting in a substantially longer Te_{A1}–Te_{A2} bond length of 3.34 Å compared to the bulk Te–Te single-bond length of 2.90 Å. As shown in Fig. 9(b), the half-filled antibonding state lies above the valence-band edge and the charge is largely localized on the Te–Te dimer along the dislocation line. The partial occupancy of the Te–Te antibonding state can be removed by alternating the dimer formation along the dislocation line as shown in Fig. 8(c). In this QP structure, the energy gain is 0.29 eV/nm with respect to the DP structure (0.43 eV/nm with respect to the SP structure), and the Te_{A1}–Te_{A2} bond length of 2.87 Å is close to the bulk single-bond length. This is associated with a charge redistribution between the Te_{A1}–Te_{A2} dimer and the threefold-coordinated Te_{A3} and Te_{A4}: 1.0e on the Te_{A1}–Te_{A2} antibonding state goes to the partially filled 5p orbitals of threefold-coordinated Te_{A3} and Te_{A4}, resulting in fully occupied 5p lone pair orbitals. Thus the Te_{A1}–Te_{A2} antibonding state is fully empty as depicted in Fig. 9(c) and is pushed toward the conduction-band edge. On the other hand, the fully occupied Te_{A1}–Te_{A2} bonding state and the 5p lone pair states of Te_{A3} and Te_{A4} lie within the valence band. With the fully occupied 5p lone pair orbitals, the threefold-coordinated Te_{A3} and Te_{A4} become more pyramidal than the partially occupied Te_{A1} in the SP configuration.

Overall, our calculations predict that the QP configuration is energetically the most favorable one compared to the DP and SP configurations for both the Cd- and Te-core 30° partial dislocations. It should be noted that core reconstruction for the 30° partial dislocation has been well studied in Si and SiC, for which the DP structure was suggested as the most probable core configuration [21,22,36]. The reason that QP configurations are favored instead in CdTe can largely be attributed to the different number of valence electrons per atom in group II-VI versus group IV compounds and the more highly polar bonds in II-VI compounds.

C. 90° partial dislocations

Next, we examine the 90° glide partial dislocation, which is the other partial associated with dissociation of the 60° glide dislocation, in addition to the 30° partial. The geometries and electronic structures of the Cd-core 90° partial dislocations are shown in Figs. 10 and 11, respectively. For the Cd-core SP structure, there are two possible geometries, distinguished by the core Cd atoms (Cd_{A1} and Cd_{B1}) being either "quasi-five-fold coordinated" with a preserved [1$\bar{1}$0] mirror symmetry as in Fig. 10(a) or fourfold coordinated with broken mirror symmetry as in Fig. 10(b); similar symmetric and asymmetric SP structures for the 90° glide partial dislocation have been reported in Si [37], SiC [22], and diamond [21]. In the symmetric structure, all the Cd_{A1}–Cd_{B1} bonds are equivalent with length 3.08 Å, while they are split into a short and a long bond with lengths 2.79 and 4.21 Å in the asymmetric structure.

As shown in Fig. 11, the PLDOS for both SP structures show a half-filled state in the middle of the band gap (0.5e

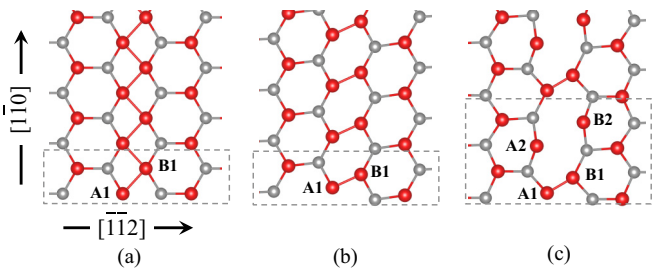

FIG. 10. Optimized configurations of a Cd-core 90° partial dislocation in the {111} glide plane. Important core Cd atoms in each unit cell are labeled as A and B with numbers, indicated. Red and gray balls represent Cd and Te atoms, respectively.

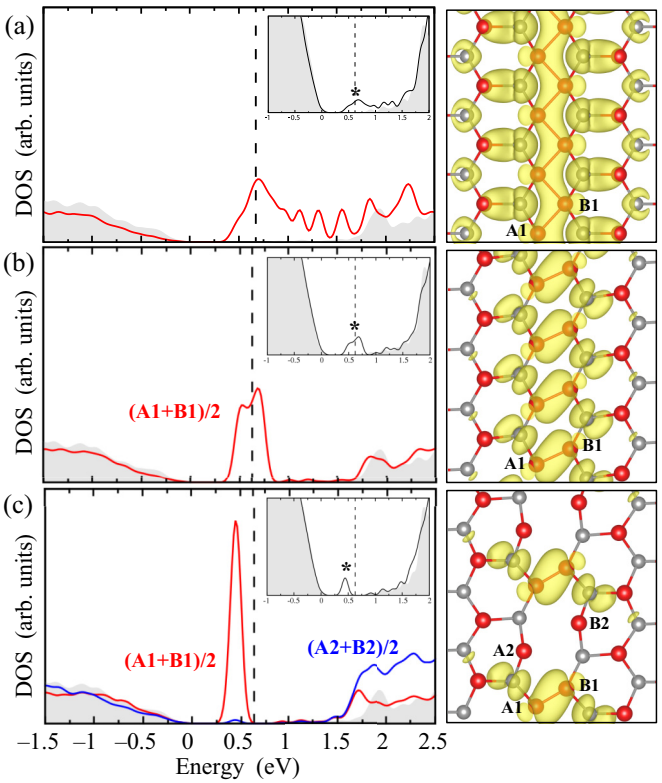

FIG. 11. (Left) Projected DOS onto the core Cd atoms and (right) band-decomposed charge density for the (a) symmetric SP (b) asymmetric SP and (c) DP core structure for the Cd-core 90° glide dislocation. The energy zero is set to the top of the valence band of the pristine structure without a dislocation, and the Fermi level is indicated by vertical dashed lines. The projected DOS onto the Cd atom in the pristine CdTe structure are shown as gray shaded areas for a reference. In the insets, the total DOS are shown by the black curves and the gray shaded areas indicate the total DOS for the reference dislocation-free CdTe structure. The band-decomposed charge densities of core-related states within the band gap (indicated by asterisks in the total DOS plot in the insets) are plotted as isosurfaces set at 10% of the maximum value.

from each broken bond associated with a core Cd atom). According to the band-decomposed charge density plots, the charge corresponding with this gap state is largely delocalized over the core Cd atoms for the symmetric structure, while it becomes more localized and resides on the Cd_{A1}–Cd_{B1} bonding state for the asymmetric structure. Our calculation predicts that the Cd-core asymmetric SP structure is slightly more stable than the symmetric one by 0.04 eV/nm, but such a small energy difference suggests no strong preference between these two SP structures. This result is in contrast to group-IV semiconductors, where the asymmetric SP structure is energetically much more favorable than the symmetric one [21,22,37]; this difference in behavior is partly due to the stronger covalent bonding interaction between group-IV atoms than between Cd atoms and also because the bonding state is fully occupied for the asymmetric dislocations in group-IV compounds since each core atom contains 1.0e from the broken bonds. The fully occupied bonding state of the asymmetric SP structure in group-IV semiconductors also yields a large energy gain, unlike the partially occupied bonding state of the Cd-core asymmetric structure in CdTe.

We find that the SP structure can undergo reconstruction into the DP structure by introducing alternating Cd_A–Cd_B bonds with an energy gain of 0.39 eV/nm. As illustrated in Fig. 10(c), the Cd_{A1}–Cd_{B1} bond length is shortened in the DP structure (to 2.64 Å) compared to that in the SP asymmetric structure (2.79 Å), indicating a stronger bonding interaction in the DP structure. On the other hand, the Cd_{A2} and Cd_{B2} atoms are widely separated, and each of these Cd atoms exhibits a nearly planar configuration with the three neighboring Te atoms. The PLDOS in Fig. 11(c) reveals that the Cd_{A1}–Cd_{B1} bonding state, which lies in the middle of the band gap, is fully occupied by the donated charge (1.0e) from the sp^2-like Cd_{A2} and Cd_{B2}. We point out that our calculated DP structure is quite different from the suggested DP structures in group-IV and III-V semiconductors [21,23]; in CdTe, the DP structure we find is 0.44 eV/nm lower in energy than the structure analogous to that found in group-IV and III-V semiconductors.[1] Such distinct DP structure for the Cd-core 90° partial dislocations can be largely attributed to the ease of formation of the sp^2-like Cd configuration by donating 0.5e to the adjacent half-filled Cd–Cd bonding state.

We further consider possible QP core reconstructions for the Cd-core 90° partial, but there is no energy gain in this case for quadruple periodicity compared to the double periodicity, unlike for the 60° and 30° cases. Since the Cd-core 90° partial in the DP structure does not have a partially filled gap state, there is no driving force for further QP core reconstruction, further demonstrating the strong correlation between core reconstructions and the electronic structure.

Finally, the core configuration for the Te-core 90° partial dislocation is shown in Fig. 12. In the symmetric SP structure, the distances between the Te_{A1} and Te_{B1} are all equivalent with length 3.58 Å. The PLDOS in Fig. 12 shows that there is a partially empty defect state near the top of the valence band. The corresponding band-decomposed charge density plot shows that the defect state is predominantly derived from the partially empty 5p orbitals of the threefold-coordinated Te_{A1} and Te_{B1}. Each broken Te bond contains 1.5e (equivalent to 0.5 hole).

We also constructed the asymmetric SP structure (not shown) by breaking the symmetry across the $[1\bar{1}0]$ mirror plane, as for the Cd-core, but the difference in structure from the symmetric one is very minor for the Te-core, with only slightly different Te_{A1}–Te_{B1} long-bond and short-bond distances of 3.50 and 3.67 Å. Accordingly, the electronic structure and energy of the asymmetric SP is very similar to that of the symmetric one for the Te core. Our calculations predict that the symmetric SP is energetically slightly more favorable than the asymmetric one, which can be understood by the antibonding nature of the Te_{A1}–Te_{B1} bond.

For the Te-core DP structures, we searched for core reconstructions associated with redistributed partial core charges, in analogy to the Te-core 30° dislocations, where partial charge from the antibonding state of one of the Te_A–Te_B goes to

[1]We took a geometry representative of the DP structure from silicon and relaxed it for CdTe to obtain the analogous DP structure.

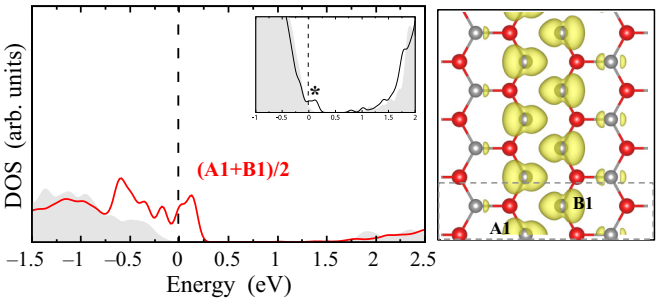

FIG. 12. (Left) Projected DOS onto the core Te atoms and (right) band-decomposed charge density for the symmetric SP core structure for the Te-core 90° glide dislocation. The energy zero is set to the top of the valence band of the pristine structure without a dislocation, and the Fermi level is indicated by vertical dashed lines. The projected DOS onto the Te atom in the pristine CdTe structure is shown as gray shaded areas for a reference. In the insets, the total DOS are shown by the black curves and the gray shaded areas indicate the total DOS for the reference dislocation-free CdTe structure. The band-decomposed charge density of core-related states within the band gap (indicated by asterisks in the total DOS plot in the insets) is plotted as isosurfaces set at 10% of the maximum value.

the partially filled $5p$ orbitals of the other Te_A and Te_B pair. However, in the Te-core 90° partial, steric inhibition of the fully occupied $5p$ orbitals of the Te_A and Te_B atoms, which face each other, prevents such a DP reconstruction from occurring. We also searched for other possible DP and QP reconstructions of the Te-core 90° dislocation, but the symmetric SP structure always is predicted to be energetically the most favorable, although the possibility of core reconstructions with larger periodicities or different stoichiometries cannot be precluded. However, a similar trend has been reported for GaAs, in which for the As-core 90° partial dislocations, the SP structure is energetically more favorable than the DP structure, whereas the DP structure is predicted to be more stable than the SP for the Ga-core 90° partial dislocation [23]. Thus our calculations suggest that the Te-core 90° partial dislocation might show metallic behavior along the dislocation line, unlike the other dislocations considered in this work.

IV. DISCUSSION

We have shown that core reconstructions along the dislocation line are energetically favorable for all isolated Cd-/Te-core 60° perfect, 30° partial, and Cd-core 90° partial dislocations in CdTe, while the Te-core 90° partial remains as the SP structure without core reconstruction along the dislocation line. The driving force for these reconstructions seems to be strongly correlated with the partially occupied core states in the SP structures, which render these dislocations metallic. Considering a dislocation as a one-dimensional (1D) like chain, such metallic behavior along the dislocation line might be unstable and a symmetry breaking that opens the band gap would be preferred, which is similar to a conjugated polymer chain that is often subject to the Peierls-like instability [38,39]. For reference, the calculated band structures for the 60° perfect (in Fig. S1 and S2), 30° partial (in Fig. S3 and S4), and 90° partial (in Fig. S5) dislocations are presented in Ref. [40]. Since the SP core states are one-quarter-filled (for the Te-core 60° and the Cd-core 30° partial) or three-quarter-filled (for the Cd-core 60° and the Te-core 30° partial) as presented in our PLDOS analysis, quadrupling the period leads to one or three fully occupied states, respectively. Indeed, our calculations show that for the the 60° perfect and 30° partial, the QP structures combine a dimer (or trimer) and a missing dimer to exhibit semiconducting characters with a modulation of the electronic density along the dislocation line. It is worth noting that formation of tetramers along the dislocation line, which might be another possible quadruply-periodic reconstruction, is highly unlikely in CdTe due to the large distance between core atoms. We also considered a possible spin ordering for the partially occupied core states in the SP structures, but it turns out that the energy of the spin-ordered SP structure is considerably higher than that of the charge-modulated QP structure for all dislocations, suggesting that spin ordering is not favorable.

Since the dislocation cores are non-stoichiometric (each Cd-core and Te-core contains excess Cd and Te atoms, respectively), the absolute formation energy of each core structure depends on the growth conditions, which determine the chemical potentials of Cd and Te atoms. Thus, the relative concentrations of Cd-core and Te-core dislocations are effected by different growth conditions; that is, Cd-core dislocations would be more favored in Cd-rich environments, and vice versa. However, the relative stabilities among the SP, DP, and QP structures for a given core type are less sensitive to the growth conditions, since they all have the same number of atoms.

In reality, different dislocations coexist in the same system, and the possibility of charge transfer between Cd-core and Te-core dislocations must be evaluated, especially for the metallic SP cores. In our calculations, when the SP Cd-core and Te-core 60° dislocations are paired together in the same system, charge transfer does occur from the Te-core (partially occupied Te_{A1}–Te_{B1} antibonding states) to the Cd-core (partially empty Cd_{A1}–Cd_{B1} bonding states). However, the total energy of this charge transfer model is still considerably higher by 0.80 eV/nm than the charge modulation model having both QP cores in the same system; for the QP cores, the electronic states of each core remain essentially the same when both Cd-core and Te-core coexist in the same system as in the isolated cases. Thus, charge modulation within the cores along the dislocation lines and the accompanying QP reconstruction would be dominant for 60° dislocations.

For the 30° partial dislocations, we find that the energy of the charge transfer model between SP Cd- and Te-cores [Fig. 13(a)] is comparable to the energy of the charge modulation model with each core QP reconstructed [Fig. 13(b)], using DFT-LDA. However, with LDA for the intracore charge modulation model, there is substantial overlap between the defect energy levels of the occupied Cd-core state and the unoccupied Te-core state within the band gap, leading to partially occupied Cd-core and Te-core states; this arises because the defect level positions within the band gap are very similar for the isolated QP reconstructed 30° Cd-core and Te-core partial dislocations, as shown in Figs. 7(c) and 9(c). Since DFT-LDA may incorrectly predict the positions of defect levels due to the underestimation of the band gap, we

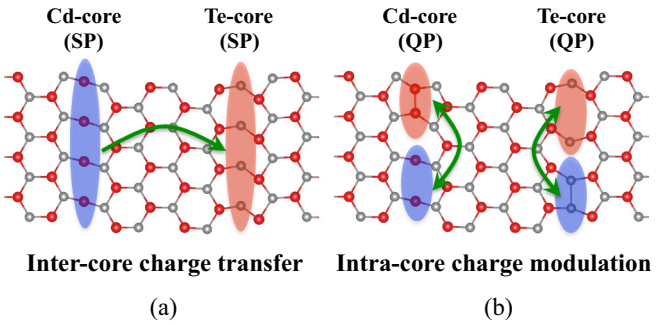

FIG. 13. Schematic representations of the (a) intercore charge transfer model and (b) intracore charge modulation model for the system having both Cd-core and Te-core 30° glide dislocations. The red and blue shaded area indicate charge accumulation and depletion, respectively, as a result of (a) the charge transfer from the Cd-core to the Te-core and (b) charge modulation accompanied by the QP core reconstruction within each core. Red and gray balls represent Cd and Te atoms, respectively.

further carried out hybrid-DFT calculations using the HSE06 functional [41] to better describe the defect level positions for the isolated QP reconstructed 30° Cd-core and Te-core partial dislocations and more accurately evaluate the energy difference between the charge transfer and charge modulation models.[2] Using the hybrid HSE06 functional, a calculated band gap of 1.6 eV was obtained, and the occupied defect state is located in the middle of the band gap for the isolated QP reconstructed Cd-core partial dislocation, while the empty defect state lies ∼0.3 eV below the conduction-band edge for the Te-core partial dislocation. Thus, with the considerable difference ($\gtrsim$0.5 eV) between the occupied Cd-core state and the empty Te-core state in the isolated systems, no overlap between these two states is expected in the combined system and complete charge modulation within each core would occur, suggesting that the energy of the intracore charge modulation model from the DFT-LDA calculation for the 30° case is considerably underestimated.[3]

In addition, the charge transfer model is only valid when the concentrations of Cd-core and Te-core dislocations are equal, and this condition may be hardly satisfied in real materials, which are usually off-stoichiometric (particularly for melt-grown material, which is ordinarily grown intentionally Te-rich). Thus intracore charge modulation with QP reconstructed cores is more likely to occur than intercore charge transfer for both 60° perfect and 30° partial dislocations.

For the 90° Te-core partial dislocation, no core reconstruction is found along the dislocation line, even though a partially occupied defect state exists, unlike the other cases studied. A possible explanation for this anomaly is that the electronic energy gain from charge redistribution is less than the strain energy cost associated with the reconstruction in this case.

Further, possible charging effects should be considered for the stabilities of the core configurations, especially for the SP structures of the partial dislocations. Since those Cd-core (Te-core) partials exhibit shallow donor (acceptor) characteristics, respectively, an adequately charged SP structure would be energetically more favorable than the neutral SP structure for intrinsic conditions of the Fermi level. The relative stability of the charged SP structure compared to the neutral QP (or DP) structure would strongly depend on the Fermi level position. For example, for the 30 partials, intracore charge modulation (representing neutral QP structures) is energetically slightly more favorable than intercore charge transfer (representing charged SP structures), which suggests that neutral Cd-core/Te-core QP structures would be more stable than positively charged Cd-core and negatively charged Te-core SP structures for intrinsic conditions. For radiation detector applications, the material is highly resistive and intrinsic conditions prevail.

Finally, we note that for the 30° partial dislocations, although the core atoms exhibit relatively large displacements along the dislocation line direction in the QP reconstructions compared to the SP cases, the atomic displacements projected onto the cross-sectional planes normal to the dislocation line are less than 0.2 Å. Thus, it would be extremely difficult to directly observe the core reconstructions experimentally, for example, with scanning transmission electron microscopy (STEM) down the dislocation line direction, even for a state-of-the-art aberration-corrected microscope [14]. Figure S6 in Ref. [40] includes STEM simulations that demonstrate the subtle, extremely difficult to resolve contrast expected for the QP cores compared to the SP cores (Ref. [43]).

V. CONCLUSIONS

We calculated the structural and electronic properties of dislocation cores for 60° glide perfect, 30° and 90° glide partial dislocations in CdTe. Semiempirical calculations were initially carried out for large dislocation models to take into account the long-range strain fields around the dislocation cores, while density functional theory (DFT) calculations were performed on smaller models extracted from the initial structures to examine core reconstructions and the associated electronic structures. For each isolated dislocation core, the singly-periodic (SP) and doubly-periodic (DP) and quadruply-periodic (QP) core configurations along the dislocation line were considered for each of the 60° Cd-/Te-core perfect and the 30° (90°) Cd-/Te-core partial dislocations. The SP cores exhibit metallic characters along the dislocation line direction with partially occupied defect states in the band gap, however, this 1-D like metallic state is highly unstable against lattice distortions along the dislocation line, in analogy with the Peierls distortion of 1-D crystal. For the 60° perfect

[2]The standard HSE06 exchange-correlation functional was used with 25% Hartree-Fock exchange and 0.2 $Å^{-1}$ long-range screening parameter. Single-shot hybrid calculations were performed using the relaxed geometries from PBE [42] calculations. For the hybrid calculations, only the Γ point was included in the Brillouin zone sampling, and an energy cutoff of 275 eV was used.

[3]Due to the computational cost, we could not directly compare energies of the intercore charge transfer model and intracore charge modulation model having both Cd-core and Te-core 30° partial dislocations together, using hybrid-DFT calculations, since those systems included 1120 atoms.

and 30° partial dislocations, we find that QP reconstructions along the dislocation line consisting of a dimer and a missing dimer in a pair are energetically the most favorable for all dislocations considered in this work. For the 90° partial dislocations, the Cd-core one prefers to be DP reconstructed, while the Te-core remains as the symmetric SP structure. The driving force for the core reconstruction can be attributed to the resulting charge modulation along the dislocation line, which produces a semiconducting character for the defect. For the QP reconstructed 60° Cd core, the fully occupied dislocation-induced defect states lie near the valence-band edge and the absence of deep defect states suggest the 60° Cd-core might not strongly trap charge carriers. For the QP reconstructed 60° Te-core, in addition to occupied states close to the valence-band edge, there are empty states below the conduction-band edge, which could affect charge transport by trapping electrons. For the 30° Cd-core (Te-core) partial dislocation, a fully occupied (empty) deep defect state appears. Accordingly, it is expected that the 30° Cd-core and 30° Te-core partial dislocations could considerably deteriorate charge transport by trapping charge carriers and inducing recombination. For the 90° Cd-core partial dislocation, a fully occupied defect state exist in the middle of the band gap, while the 90° Te-core induces partially empty defect state near the valence-band top. Lastly, we compare the energetics between intercore charge transfer and intracore charge modulation when two different cores are paired together. For the 60° cores, when a Cd and Te cores are paired together they strongly prefer to maintain intracore charge modulation with individual QP reconstructions rather than transfer charge between them. However, the energetics for the intracore charge modulation compared to intercore charge transfer are very close for the 30° Cd-/Te-cores, although in real material, the intracore charge modulation should be more likely due to constraints on the intercore charge transfer occurring.

ACKNOWLEDGMENTS

This work was performed under the auspices of the U.S. Department of Energy by Lawrence Livermore National Laboratory under Contract DE-AC52-07NA27344, with support from the DOE National Nuclear Security Administration Office of Defense Nuclear Nonproliferation Research and Development (project LL13-MatModelRadDetect-PD3YJ). Helpful contributions by Eunae Cho and Michael Skarlinski are warmly acknowledged.

[1] T. Takahashi and S. Watanabe, IEEE Trans. Nucl. Sci. **48**, 950 (2001).
[2] T. Schlesinger, J. Toney, H. Yoon, E. Lee, B. Brunett, L. Franks, and R. James, Mater. Sci. Eng., R **32**, 103 (2001).
[3] A. Castaldini, A. Cavallini, B. Fraboni, L. Polenta, P. Fernandez, and J. Piqueras, Phys. Rev. B **54**, 7622 (1996).
[4] M. Amman, J. S. Lee, and P. N. Luke, J. Appl. Phys. **92**, 3198 (2002).
[5] C. Szeles, W. C. Chalmers, S. E. Cameron, J.-O. Ndap, M. Bliss, and K. G. Lynn, in *International Symposium on Optical Science and Technology* (International Society for Optics and Photonics, 2001), pp. 57.
[6] V. Lordi, J. Cryst. Growth **379**, 84 (2013).
[7] A. E. Bolotnikov *et al.*, IEEE Trans. Nucl. Sci. **56**, 1775 (2009).
[8] V. Babentsov, V. Boiko, G. Schepelskii, R. James, J. Franc, J. Prochazka, and P. Hlidek, J. Lumin. **130**, 1425 (2010).
[9] V. Babentsov, V. Boiko, G. Schepelskii, R. James, J. Franc, J. Prochazka, and P. Hlidek, Nucl. Instrum. Methods Phys. Res., Sect. A **633**, S81 (2011).
[10] C. Buis *et al.*, Nucl. Instrum. Methods Phys. Res., Sect. A **735**, 188 (2014).
[11] S. Mahajan and L. Kimerling, *Concise Encyclopedia of Semiconducting Materials and Related Technologies* (Elsevier, 2013).
[12] A. Blumenau, T. Frauenheim, S. Öberg, B. Willems, and G. Van Tendeloo, in *Defect and Diffusion Forum* (Trans Tech Publ, 2004), Vol. 226, pp. 11.
[13] S. Takeuchi and K. Suzuki, Phys. Status Solidi A **171**, 99 (1999).
[14] C. Li, Y. Wu, T. J. Pennycook, A. R. Lupini, D. N. Leonard, W. Yin, N. Paudel, M. Al-Jassim, Y. Yan, and S. J. Pennycook, Phys. Rev. Lett. **111**, 096403 (2013).
[15] C. Li, J. Poplawsky *et al.*, Ultramicroscopy **134**, 113 (2013).
[16] T. Paulauskas, C. Buurma, E. Colegrove, B. Stafford, Z. Guo, M. K. Chan, C. Sun, M. J. Kim, S. Sivananthan, and R. F. Klie, Acta Crystallogr. Sect. A **70**, 524 (2014).
[17] P. Lu and D. J. Smith, Philos. Mag. B **62**, 435 (1990).
[18] D. B. Holt and B. G. Yacobi, *Extended Defects in Semiconductors: Electronic Properties, Device Effects and Structures* (Cambridge University Press, 2007).
[19] L. Pizzagalli, J. Godet, and S. Brochard, Phys. Rev. Lett. **103**, 065505 (2009).
[20] K. Zhong, Q. Meng, and W. Zhao, Phys. Status Solidi B **249**, 1250 (2012).
[21] A. T. Blumenau, M. I. Heggie, C. J. Fall, R. Jones, and T. Frauenheim, Phys. Rev. B **65**, 205205 (2002).
[22] G. Savini, M. I. Heggie, and S. Öberg, Faraday Discuss. **134**, 353 (2007).
[23] S. Beckman and D. Chrzan, Phys. Status Solidi B **243**, 2122 (2006).
[24] Z. Q. Wang, D. Stroud, and A. J. Markworth, Phys. Rev. B **40**, 3129 (1989).
[25] S. Plimpton, J. Comput. Phys. **117**, 1 (1995).
[26] D. M. Ceperley and B. J. Alder, Phys. Rev. Lett. **45**, 566 (1980).
[27] P. E. Blöchl, Phys. Rev. B **50**, 17953 (1994).
[28] G. Kresse and J. Furthmüller, Phys. Rev. B **54**, 11169 (1996).
[29] H. J. Monkhorst and J. D. Pack, Phys. Rev. B **13**, 5188 (1976).
[30] R. W. G. Wyckoff, *Crystal Structures*, Vol. 1 (Interscience, 1960), p. 331.
[31] E. Menéndez-Proupin and W. Orellana, Phys. Status Solidi B **252**, 2649 (2015).
[32] D. Åberg, P. Erhart, and V. Lordi, Phys. Rev. B **88**, 045201 (2013).
[33] S. Wippermann, M. Vörös, A. Gali, F. Gygi, G. T. Zimanyi, and G. Galli, Phys. Rev. Lett. **112**, 106801 (2014).

[34] P. Brown and J. Forsyth, Acta Crystallogr. Sect. A **52**, 408 (1996).
[35] S. Öberg, Phys. Status Solidi B **108**, 357 (1981).
[36] F. Bernardini and L. Colombo, Phys. Rev. B **72**, 085215 (2005).
[37] J. R. K. Bigger, D. A. McInnes, A. P. Sutton, M. C. Payne, I. Stich, R. D. King-Smith, D. M. Bird, and L. J. Clarke, Phys. Rev. Lett. **69**, 2224 (1992).
[38] R. E. Peierls, *Quantum Theory of Solids* (Oxford University Press, 1955), Vol. 23.
[39] A. Moliton and R. C. Hiorns, Polym. Int. **53**, 1397 (2004).
[40] See Supplemental Material at http://link.aps.org/supplemental/10.1103/PhysRevB.93.174109 for the calculated band structures.
[41] J. Heyd, G. E. Scuseria, and M. Ernzerhof, J. Chem. Phys. **118**, 8207 (2003).
[42] J. P. Perdew, K. Burke, and M. Ernzerhof, Phys. Rev. Lett. **77**, 3865 (1996).
[43] See Supplemental Material at http://link.aps.org/supplemental/10.1103/PhysRevB.93.174109 for the simulated STEM images.